Chemical Thermodynamic Insights on Rare-Earth Magnet Sludge Recycling

Citation: Wagner, Mary-Elizabeth and Antoine Allanore. "Chemical Thermodynamic Insights on Rare-Earth Magnet Sludge Recycling." ISIJ International 60, 11 (November 2020): 2339-2349. © 2020 The Iron and Steel Institute of Japan

As Published: http://dx.doi.org/10.2355/isijinternational.isijint-2020-320

Publisher: Iron and Steel Institute of Japan

Persistent URL: https://hdl.handle.net/1721.1/131075

Version: Final published version: final published article, as it appeared in a journal, conference proceedings, or other formally published context

ISIJ International, Vol. 60 (2020), No. 11, pp. 2339–2349
https://doi.org/10.2355/isijinternational.ISIJINT-2020-320

Chemical Thermodynamic Insights on Rare-Earth Magnet Sludge Recycling

Mary-Elizabeth WAGNER and Antoine ALLANORE*

Massachusetts Institute of Technology, 77 Massachusetts Avenue, Office #13-5095, Cambridge, Massachusetts, 02139 USA.

(*Received on June 2, 2020; accepted on June 25, 2020*)

Recycling rare-earth magnets poses a metallurgical challenge due to their high reactivity and the difficulty in separating individual rare-earth elements. These challenges are compounded when considering magnet machining sludge, which is more heavily oxidized and contains more contaminants than typical end-of-life magnets. If recycled, these materials are sent back to the primary smelter, where they are separated and purified to make new feedstocks which are often re-mixed into a new magnet. Here, a thermodynamic study is presented, assessing the oxidation behavior of rare-earth magnets. The theoretical minimum energy to reduce the whole magnet sludge, without separation and purification, is also presented. A comprehensive model including 25 elements is provided, using a hybrid CALPHAD-classical method. Oxygen distribution in a rare-earth magnet, with a total O content ranging between 0.09% to 5.4 wt%, is assessed. The results predict a final distribution of 40 wt% rare-earth in the oxide phase, with 60 wt% still remaining in the metallic phase. The model performance with respect to published experimental data is used to shed light into the possible processing methods for recycling.

KEY WORDS: rare-earth magnets; recycling; thermodynamic modeling; oxidation; reduction; magnet sludge.

1. Introduction

Rare-earth magnets of the Fe–R–B type (iron, rare-earth, boron) are becoming increasingly popular for their use in everything from small electronics to turbines. The rare-earth elements in these magnets are alloyed to achieve a composition of more than 60% iron, producing an iron-rich microstructure not unlike that of hypoeutectoid steel. In place of pearlite, the large grains are an Fe–R–B compound phase, called the 2-14 phase for its stoichiometry: $Fe_{14}R_2B$. The 2-14 grains are separated not by ferrite, but by a metallic rare-earth rich solid-solution grain boundary phase.[1,2] **Figure 1** shows a schematic of the typical microstructure found in an Fe–R–B type magnet. Unlike pearlitic steel, this alloy must be rapidly quenched for this microstructure to appear: at low temperature an iron solution is favored over the $Fe_{14}R_2B$ compound. If processed correctly, this iron-based alloy has demonstrated unique bulk magnetic performances, creating the opportunity to miniaturize magnets for extremely powerful magnetic fields. **Figure 2** gives an overview of the main processing steps involved in Fe–R–B magnet manufacturing. Ultimately, the cast alloy is jet milled into a fine powder and sintered into its final form. Magnet production, therefore, incorporates many areas of ferrous metallurgical knowledge, from casting to powder metallurgy. At the core of this process is the composition of the cast alloy. This composition dictates the elemental distribution in the final microstructure, and in turn, the magnetic performance. As in high-end steel production, elemental compositions are controlled below a fraction of a weight percent at casting and problematic impurities like Si and P are kept to an absolute minimum.

In its methods of casting, powder metallurgy, and impurity control, the magnet manufacturing industry drew inspi-

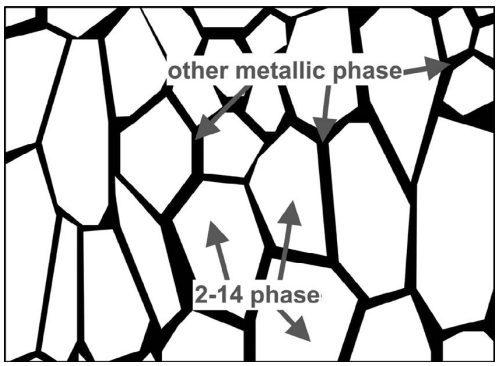

Fig. 1. Schematic of a typical Fe–R–B magnet microstructure showing the magnetic 2-14 grains separated by a rare-earth rich "other metallic phase" at the grain boundaries.

* Corresponding author: E-mail: allanore@mit.edu

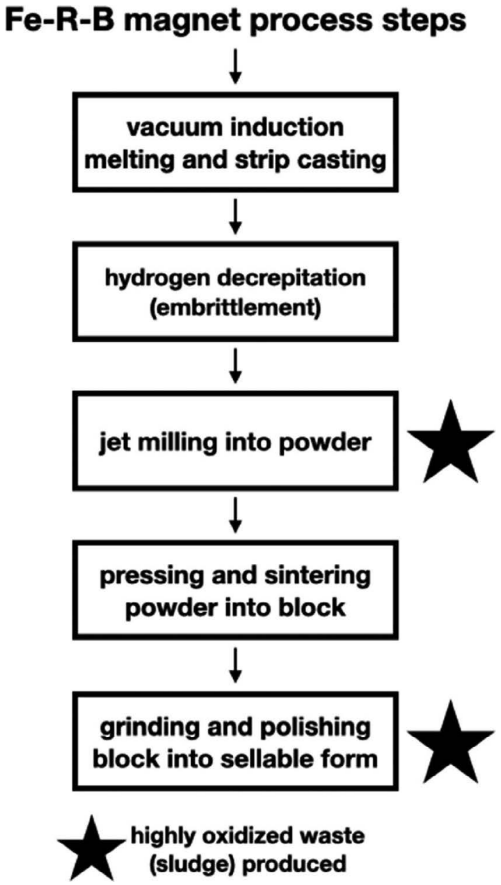

Fig. 2. Overview of main processing steps in Fe–R–B magnet production. Highly oxidized waste such as magnet sludge is produced mainly during the jet milling and machining steps.

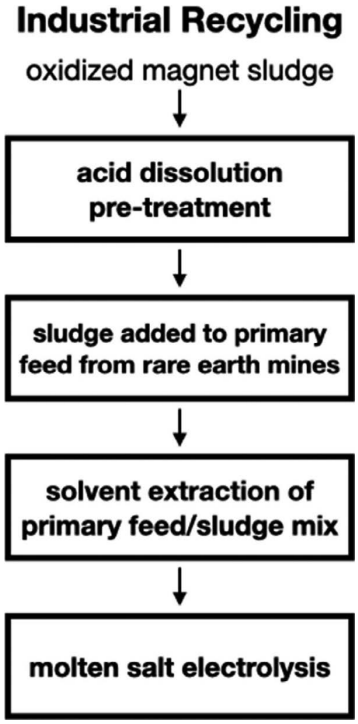

Fig. 3. Overview of the current magnet sludge recycling process. Commercial magnet sludge recycling occurs at the primary rare-earth smelter.

ration from the technology of the steel industry to improve and expand. At the same time, the demand increased for rare-earth metals, which have a supply pipeline and market very different from steel because primary production occurs mostly in one country, China. Because most rare-earth mines and smelters are concentrated in this single country, the market is exposed to the political, environmental, and social risks that arise from not having sufficient alternative sources readily available in other regions of the world.[3,4] In addition to the geographical limitations of mining and processing rare-earths, their chemistry provides other challenges. The rare-earths are f-block metals, and can be divided into two subgroups: light rare-earths (lanthanum through samarium) and heavy rare-earths (europium through lutetium). Elements within these subgroups are known for their chemical similarity- a trait that makes separating these elements difficult. Producing purified rare-earths in a primary smelter is expensive, energy intensive, and creates radioactive and acidic waste that require extensive treatment to mitigate their environmental impact.[4] Downstream from primary production, the development of ever newer, smaller, and faster electronics pushes for more virgin material to be mined and processed. Considering these circumstances, magnet recycling is essential in order to decouple primary rare-earth mining from the production of rare-earth magnets.

Most efforts for magnet recycling focus on bulk magnet waste, which comes from large decommissioned equipment such as turbines. Typically still in one piece, their contamination is often limited to their surface and they have not reacted much with oxygen. Beyond the traditional hydrometallurgical recycling methods, hydrogen reduction,[5,6] chlorination,[7] metallothermic reduction with calcium (Ca)[8] and phase separation with liquid magnesium (Mg)[9] have been proposed, among others.[3] Magnet sludge created when manufacturing smaller magnets is more difficult to treat. This is the highly oxidized factory waste produced during jet milling, machining, and grinding magnets down to their final sellable form (Fig. 2). Magnet sludge is different from bulk end-of-life magnets. It has higher levels of oxygen alongside other contaminants from machining, such as carbon from lubrication. If magnet sludge is recycled, its high levels of oxygen and other impurities mean it is treated similarly to a mined rare-earth ore. **Figure 3** outlines this commercial recycling process. The sludge is first cleaned with acid before being sent back to primary rare-earth smelters where it is mixed with mined ore prior to solvent extraction. Ultimately, pure rare-earth metals are obtained via molten salt electrolysis.[3] During the leaching step, all of the sludge is oxidized, including portions that may have originally still been metallic. Additional energy is required to re-reduce these metals to create suitable rare-earth metal or alloy feedstock. Despite the challenge of being highly contaminated, efforts have been made to develop a recycling process targeted specifically at magnet sludge. Research into these new methods mostly focus on Ca reduction because of the sludge's high oxygen levels.[8,10–13]

Recycling sludge by mixing with primary feed aims at recovering the rare-earth metal value, and the end goal is to obtain a purified product that can be sold to downstream production companies like magnet manufacturers. This strategy may be criticized with two sustainability arguments. First, if the goal of recycling is to avoid the environmental

and economic costs of primary rare-earth production, treating sludge alongside primary feed will link the secondary rare-earth content value to the primary rare-earth value. This is analogous to the connection between scrap steel price and primary steel price. Second, the rare-earth sludge is treated as a type of rare-earth ore, when in fact, at greater than 60 wt% Fe, the sludge is closer in elemental composition to a heavily oxidized scrap iron alloy.[13,14)]

With these two arguments in mind, we consider sludge and magnet manufacturing wastes as iron-based materials with essentially the correct metal composition needed to produce a magnet. We herein model the underlying chemical thermodynamics aiming producing a magnet directly from such wastes. In order to explore this iron-based perspective of sludge recycling, a comprehensive thermodynamic assessment is proposed. First, we modeled the reaction of magnet sludge with oxygen and second, we estimated the reduction energy needed to remove this oxygen and return the magnet back to its original composition. Although magnet sludge is also contaminated by cutting media and lubricant, studies dedicated to sludge recycling have shown promising results in cleaning away these impurities, which are not typically chemically bonded to the magnet.[11,13)] Since oxygen chemically reacts with the metals in the magnet, it poses a true chemical metallurgy challenge to recycling. Thus, treating oxygen is the focus of this work.

A popular modeling approach is to use the CALPHAD (CALculation of PHAse Diagrams) method. This would require optimized databases of Gibbs energy of the relevant elements in their pure form, as well as in the solution phase (known as a solution model). The more data fed into the optimization software, the more "robust" the database will be, and the more accurate its predictions. As of today, rare-earth magnet systems do not have a completed solution database that has been published. This is in contrast to most iron alloys, which have detailed solution models developed specifically by and for the steel industry. Although building a CALPHAD model for the rare-earth magnet system is ongoing,[15–21)] so far published models are limited to specific cases, such as Fe–Pr–B or Fe–Nd–B, with limited integration of multiple rare-earth elements alongside iron and boron. The case is further complicated by a lack of a solution model able to accommodate both additives (*e.g.* Al, Ga, Nb) as well as impurities (*e.g.* C, O, S).

In absence of a solution model able to accommodate all elements present in a typical magnet, a hybrid CALPHAD-classical approach was developed. Thermodynamic calculations herein involve only standard state Gibbs energies of pure components and compounds. Using standard state to study oxidation has a rich history in ferrous thermodynamics in the form of Ellingham and Kellogg diagrams, which both relate the oxidation behavior of a pure metal or compound to the atmosphere and temperature of its environment.

2. Methodology

2.1. Thermodynamic Model

The "Equilib" module of FactSage 7.3 was used to minimize the Gibbs energy and predict which pure components and compounds were stable under a set of given conditions (*e.g.* temperature and pressure). The standard-state elements and compounds used were divided into three phase subgroups:

1. the magnetic "2-14" phase consisting of $Fe_{14}R_2B$ where R may be Pr, Nd, or Dy;

2. the "other metallic" phase, which consists mostly of rare-earths along with additives and impurities that make up the intergrain region between the 2-14 phase[1,22)]

Table 1. Modeled Gibbs energy of 2-14 compounds modified to limit reaction with oxygen.

Phase	T-Range (K)	ΔG (T)
$Fe_{14}Pr_2B$	298.15–500	−489 604.7 + 2 668.6*T − 491.2*TlnT + 8.3E−02*T^2 − 5.1E−05*T^3 + 3 334 946.8*T^{-1} − 62 399 762*T^{-2}
	500–800	−466 493 + 2 120.4*T − 399.1*TlnT − 7.3E−02*T^2 − 3.3E−06*T^3 + 2 320 237.7*T^{-1} − 62 399 762*T^{-2}
	800–1 068	−261 189.6 − 191.5*T − 59.8*TlnT − 0.3*T^2 + 3E−05*T^3 − 20 855 972*T^{-1} − 62 399 762*T^{-2}
	1 068–1 204	−1 415 268.7 + 10 423.7*T − 1 565.5*TlnT + 0.5*T^2 − 6.3E−05*T^3 + 1.4E+08*T^{-1} − 62 399 762*T^{-2}
	1 204–1 811	−492 027.2 + 2 410.9*T − 439.3*TlnT − 6.3E−02*T^2 − 8.3E−07*T^3 + 2 320 237.7*T^{-1} − 62 399 762*T^{-2}
	1 811–1 812	−849 221.2 + 4 855.8*T − 754.1*TlnT − 1.5E−03*T^2 + 1 237 197.8*T^{-1} − 62 399 762*T^{-2}
	1 812–2 350	317 721.9 − 619.7*T − 110.1*TlnT − 1.5E−03*T^2 + 1 237 197.8*T^{-1} − 62 399 762*T^{-2}
	2 350–2 800	316 246.8 − 615.1*T − 110.6*TlnT − 1.4E−03*T^2 + 1 830 376.6*T^{-1}
	2 800–3 000	397 703.3 − 843.8*T −85.9*TlnT
$Fe_{14}Nd_2B$	200–450	−491 095.8 + 2 024.7*T − 360.1*TlnT − 0.3*T^2 + 4.1E−05*T^3 − 1 226 885.5*T^{-1}
	450–576	−3 359 228.3 + 63 255.1*T − 10 474*TlnT + 15.5*T^2 − 4.6E−03*T^3 + 1.5E+08*T^{-1}
	576–618	−9 697 023.9 + 264 314.3*T − 44 496.2*TlnT + 69.7*T^2 − 1.8E−02*T^3
	618–3 000	−462 765.3 + 2 524.3*T − 470*TlnT
$Fe_{14}Dy_2B$	298–450	2.2E + 13 − 1.1E+11*T − 360.1*TlnT − 0.3*T^2 408 333.3*T^3 + 1.2E−04*T^{-1}
	450–592	−5.3E + 13 + 1.4E+11*T − 10 474*TlnT + 15.5*T^2 − 4.6E−03*T^3 + 1.5E+08*T^{-1}
	592–616	−5.3E + 13 + 1.4E+11*T − 44 496.1*TlnT + 69.7*T^2 − 1.8E−02*T^3
	616–3 000	−5.3E + 13 + 1.4E+11*T − 470*TlnT

real stoichiometry: Fe(14.00018) RE(1.99988) B(0.9994)

3. any oxides present.

The "other metallic" phase was modeled using the FactPS database in FactSage,[23] with the exception of R–B compounds, R–Fe compounds, and non 2-14 Fe–R–B compounds. The oxide phase was modeled using FactPS and Fe–R–B–O compounds optimized by Jakobsson *et al.*[21] The 2-14 phase has been reported to initially oxidize less than other magnet components.[24,25] This limited oxidation did not appear to be accounted for in published thermodynamic models,[16–18] and so herein is assumed to be of a kinetic origin. In order to account for this behavior and add this constrain on phase stability, the $\Delta H_{formation}$ for $Fe_{14}Pr_2B$, $Fe_{14}Nd_2B$, and $Fe_{14}Dy_2B$ were modified from their originally optimized values.[16–18] For each compound, $\Delta H_{formation}$ was lowered by increments of 10 kJ until overall 2-14 phase formation was favored over competing Fe-intermetallics, *e.g.* Fe_2Ti. The Gibbs energy functions for the modified compounds are presented in **Table 1**.

2.2. Initial Melting of the Rare-earth Magnet

As most magnet producers use proprietary concentrations of rare-earths and additives, a detailed compositional analysis of feedstock for magnet production could not be found. Lixandru *et al.*[14] measured the major and minor elements contained in laptop speaker magnet waste through ICP-OES: Fe, Nd, Pr, Dy, Gd, Co, Nb, Cu, Al, Ga, Zn, B. The average composition measured fell within the range suggested by prior art.[1] These published results inform the basis of the present case study. In order to include the contribution of impurities, four main feedstocks were identified: electrolytic iron, ferroboron, ferroniobium, and praseodymium-neodymium alloy. Commercial sources of these feedstocks often disclose the composition of impurities such as O and C, and impurity levels often vary depending on feed grade and source. The commercial sources used in this study were chosen on the basis of report thoroughness and overall purity: a source that disclosed O, C, Si, and P content would be chosen over a source that only disclosed C content. When deciding between two equally well-detailed sources, the one with the lowest impurity content was chosen to reflect a magnet manufacturing strategy based on premium material grades. The impurity compositions found in this manner were then added to the total mass balance.[26–28] This method worked well for all elements except for Si and P. Their estimated weight percent in the initial mass balance was so high they impeded formation of the 2-14 phase, and as such their amounts in the final mass balance were reduced to 10% of their originally estimated value. From a ferrous metallurgy consideration, it can be assumed that advanced magnet producers would source specialty feed low in Si and P content. Gd, Dy, Cu, Al, Ga, Zn, and Co were present at such low concentration that any impurities in their respective feedstock were neglected. **Table 2** summarizes the composition of the feedstocks and initial input used in this case study.

This initial input was allowed to equilibrate at 1 723 K and 0.5 bar Ar containing 1 ppm O_2, CO and H_2O; and 5 ppm N_2[29] using FactSage's Equilib software. This step simulated the conditions in the vacuum induction melting (VIM) furnace, the first step in magnet production. Temperature and atmospheric conditions were taken from prior art.[1,22] The results after the melting step are presented in Table 2. This high temperature step refined the magnet composition, as species were allowed to volatilize off and react with oxygen impurities in the Ar atmosphere.

Table 2. Elemental compositions used for calculations with no additional oxygen. Initial: compositions estimated from published reports. Post-VIM: calculated after "initial" composition equilibrated at 1 723 K to simulate treatment in vacuum induction melting furnace.

Element	Initial (wt%)	Post-VIM (wt%)
Pr	6.69%	6.72%
Nd	23.46%	23.59%
La	0.02%	0.02%
Ce	0.02%	0.02%
Fe	65.06%	65.41%
Al	0.66%	0.66%
Si	0.01%	0.01%
Mo	0.02%	0.02%
W	0.02%	0.02%
Ti	0.02%	0.02%
Ca	0.003%	0.002%
Mg	0.01%	0.00%
S	0.01%	0.01%
C	0.02%	0.02%
B	0.96%	0.96%
P	0.01%	0.01%
Mn	0.06%	0.05%
Cr	0.005%	0.005%
O	0.09%	0.09%
Nb	0.05%	0.05%
Ta	4E-5%	4E-5%
Dy	1.67%	1.67%
Gd	0.06%	0.06%
Co	0.44%	0.45%
Cu	0.12%	0.12%
Ga	0.05%	0.04%
Zn	0.50%	0.00%

2.3. Strip Casting Kinetic Simulation

In practice, as illustrated in **Fig. 4**, after a magnet is melted in the VIM, it is rapidly cooled via strip casting. This rapid cooling inhibits the formation of ferrite and promotes the 2-14 phase instead. As in other rapid cooling methods of ferroalloys, carbon rejection and graphite precipitation are also prevented. The lack of ferrite and graphite creates a metastable alloy. FactSage allows for modeling of kinetically metastable phases by enabling the user to "de-select", or suppress certain phases. If suppressed, the "de-selected" phase will not form and the next stable phase will form instead. An instructive example can be seen in steel modeling. If graphite is suppressed, cementite will form instead. To obtain the metastable phases created through rapid cooling, herein all pure Fe and pure C phases were selected as "suppressed" phases and were not allowed to form. This led to the formation of iron compounds and carbides. To further simulate rapid cooling, no gas evolution was allowed. It was

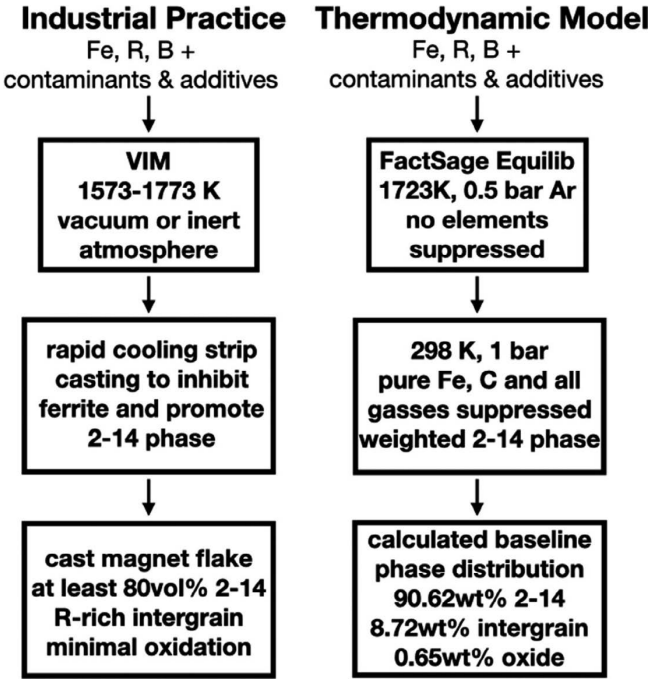

Fig. 4. Comparison between actual magnet manufacturing (left) and the modeling steps used herein (right).

at this point in the model that the modified 2-14 compounds were incorporated in order to account for their kinetic stability. A full comparison between industrial practice and our results is presented in Fig. 4.

2.4. Oxidation Model

Rare-earth metals are very reactive with oxygen. High oxygen content is one of the main barriers to effective magnet sludge recycling. For this reason, we modeled how oxygen uptake by the magnet affected its phase composition and recyclability.

The elemental oxygen content in the condensed phases present post-furnace were incrementally increased, with a total O content ranging from 0.1 wt% to 5.4 wt%. The ratios of all other elements were kept constant. New phases were calculated using Equilib at 298 K with gas phases and all pure Fe and C phases suppressed. The kinetically modified 2-14 compound data were used, and the $Fe_{14}Pr_2B$ phase was suppressed. As this metastable phase was not predicted form in the initial case without added oxygen, it could not reasonably form on its own at 298 K with an increase in oxygen. Because the model was based in standard-state thermodynamics using only compounds and pure elements, no model for dissolved oxygen was used. All oxygen was modeled as incorporated in an oxide compound phase.

2.5. Oxygen Removal

Our recycling study aims at oxygen removal from sludge in order to re-create a usable magnet with the correct chemical composition. In order to remove oxygen, here modeled as oxide compounds, it was necessary to calculate the chemical (Gibbs) energy required to reduce the oxide phases to metal and oxygen gas. This $\Delta G_{reduction}$ decreases with increasing temperature for metal oxides. This energetic benefit with temperature is offset by the energy (enthalpy) cost of heating the sludge, ΔH_{heat}. Both $\Delta G_{reduction}$ and ΔH_{heat} were calculated for this study. First, condensed phases obtained from the 5.4 wt% oxidation model were allowed to reach internal equilibrium at room temperature. Pure Fe and pure C phases were allowed, and unweighted 2-14 phases were used. This simulated the changes in the sludge during the pre-reduction steps and heating from room temperature to the target reduction temperature. At a finite temperature above room temperature, it is expected that the oxidized sludge will reach internal equilibrium, redistributing C, O, Fe, and R across the most stable phases. Once equilibrated, ΔH_{heat} was calculated as the energy required to heat the newly equilibrated material to processing temperature. $\Delta G_{reduction}$ was found as the energy required to completely decompose the oxidized sludge to metal + (O, O_2, and O_3) at the processing temperature. Other gas phases such as CO, CO_2, and SO_2 were also permitted, but gaseous metal oxides were not. When calculating the amount of energy needed to remove O completely from the magnet, 5.4 wt% O was chosen as the starting total oxygen content in the sludge. This level was similar to experimentally measured values available in the literature.[11,13,30]

3. Results

3.1. Simulated Magnet after Melting and Casting

The output from the VIM model at 1 723 K and 0.5 bar Ar shows minor changes to the overall magnet composition. Most notably, all of the Zn and Mg were predicted to volatilize off. Starting with one tonne of initial feedstock, 107 g Mn, 64 g Ga, 11 g Dy, 9 g Ca, 3 g Cu, and 2 g Nd also volatilized off. This new composition (Table 2) was then used to calculate the baseline phase distribution.

Figure 5 shows the calculated weight percent of each phase (oxide, 2-14, and "other metallic") and **Fig. 6** shows the distribution of each rare-earth element among these three phases. The oxide phase, present overall at 0.65%, is comprised of Gd_2O_3 and Nd_2O_3. The 2-14 phase, at 90.63%, consists of $Fe_{14}Nd_2B$ and $Fe_{14}Dy_2B$. Finally, the "other metallic" phase, with the remaining rare-earth and boron, additives, and impurities, contains GdS, Ce_2C_3, Nd_2B_5, LaC_2, Pr, Nd, and $PrAl_2$, among other non-rare-earth containing compounds. Appendix (Table A1) details the model inputs and outputs at each stage in the baseline calculation.

3.2. Addition of Oxygen

After equilibration in the VIM, the baseline percentage of oxygen in the as-cast magnet was estimated to be 0.09 wt% O. Oxygen was incrementally added to the magnet until 5.4 wt% O was achieved. As the oxygen content increases, the predicted phase distribution changes, as presented in **Fig. 7**. The rare-earth elements in the "other metallic" phase oxidize at the lowest levels of oxygen, converting into oxide until the "other metallic" phase drops from 8.1% to 0.8 wt% at 1.8% O. At this oxygen level, the 2-14 phase begins to decompose into oxide and various metallic phases. Appendix (Table A2) details the inputs and outputs at each stage in the calculation for the case of 0.1% O. The 2-14 phase continued to decrease with increasing O, until it became the minor phase: 15.2% at 5.4%O.

Figure 8 shows that for an oxygen content of 5.4%, the distributions of rare-earths among the phases change sig-

Fig. 5. Calculated phase distribution in the simulated magnet after melting and casting with no additional oxygen added (baseline case). (Online version in color.)

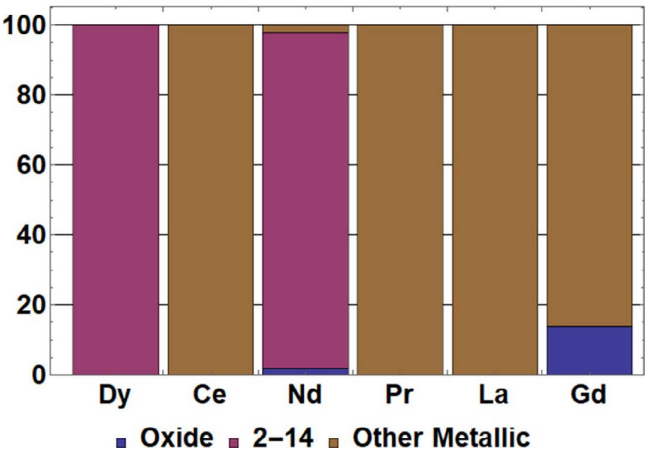

Fig. 6. Modeled distribution of rare-earth elements among phases in baseline case. Rare-earth containing phases present: Dy: 100% $Fe_{14}Dy_2B$, Ce: 100% Ce_2C_3, Nd: 2% Nd_2O_3, 96% $Fe_{14}Nd_2B$, 2% Nd_2B_5 Pr: 82% Pr and 18% PrA_{12}, La: 100% LaC_2, Gd: 14% Gd_2O_3, 86% GdS. (Online version in color.)

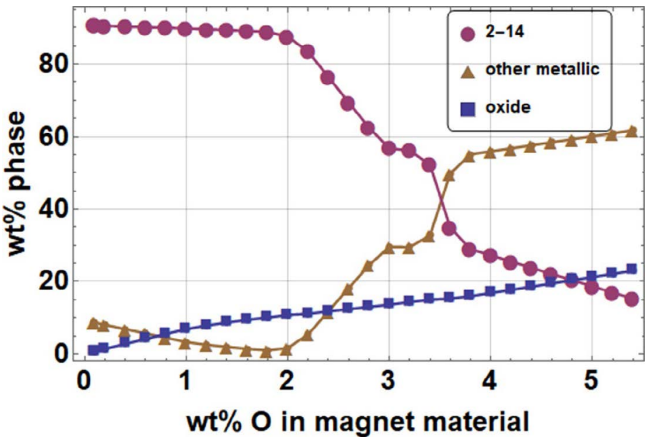

Fig. 7. Calculated changes in phases present as oxygen content is increased from 0.09 wt% to 5.4 wt%. ●: 2-14 phase, ▲: "other metallic" grain boundary phase, ■: oxide phase. After the grain boundary phase is completely oxidized near 1.8 wt%, the 2-14 phase begins to break down into oxide and more metallic phases. (Online version in color.)

nificantly from the baseline case (Fig. 6). The heavy rare-earths, Dy and Gd, are completely oxidized, while some of the lighter rare-earths, most notably Nd and Pr, remain in a metallic state. Overall, 40% of the rare-earth elements by weight are oxidized, while 60% remain in the metallic phase.

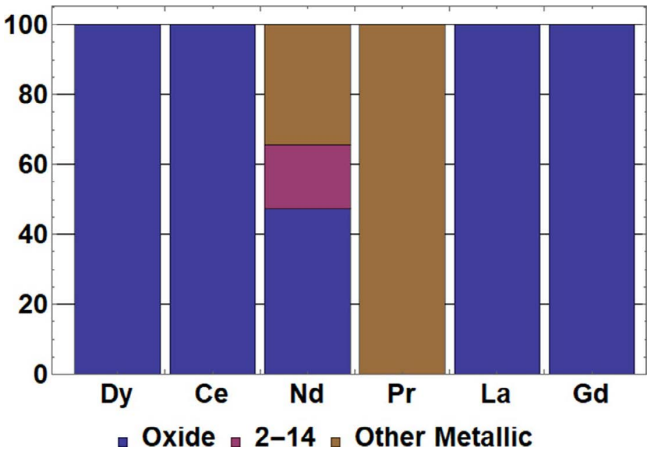

Fig. 8. Modeled distribution of rare-earth elements among phases with 5.4 wt% O present. Rare-earth containing phases present: Dy: 100% $Dy_3Al_5O_{12}$ Ce: 15% CeO_2 85% $CeCrO_3$ Nd: 2% $Nd_3Al_5O_{12}$, 45% $NdBO_3$, 18% $Fe_{14}Nd_2B$, 35% Fe_8Nd Pr: 100% Fe_8Pr Gd: 100% $Gd_3Al_5O_{12}$ (Online version in color.)

3.3. Reduction Thermodynamics

A study of the energy needed to reduce all of the oxides contained in the 5.4 wt% O case was conducted. Two different case studies were considered:

1) the energy to heat and reduce *only* the rare-earth oxides initially contained in magnet sludge, assuming that the rare-earth oxides were first separated from the rest of the waste prior to treatment.

2) the energy to heat and reduce 1 tonne of simulated waste material at 5.4 wt% O.

Figure 9 compares these two cases, looking first at the ΔG to reduce the material and second at how ΔH influences the energy requirements. For consistency, all cases have been normalized by the mass of oxidized rare-earth metal present in each case. This normalization was chosen so the results could be easily compared with analyses of current recycling methods.[4,31] For Case 1, which models the case where rare-earth oxides would be first separated from the magnet before reduction, the amount of oxidized rare-earth is fixed at 0.123 tonne RE/tonne waste. For Case 2, which models the entire magnet waste (including rare-earth metals not oxidized initially due to kinetics), the amount of oxidized rare-earth at equilibrium varies with temperature. It can be seen in Fig. 9 that less energy is needed to reduce the rare-earth oxides if reduced alongside the rest of the magnet waste than to reduce the rare-earth oxides alone. This is true regardless if ΔH is considered. If ΔH is considered, the benefit to reducing the entire magnet waste is lessened at higher temperatures as more energy is expended to heat the whole magnet as opposed to just the oxidized fraction. Above 2 000 K a crossover point will occur where it is more energetically favorable to treat only the oxides.

Figure 10 shows the phase distribution at 1 773 K as simulated magnet waste is deoxidized from 5.4%O to 0%. Fe-rich metallic phases containing no rare-earths and oxide phases containing mostly rare-earth oxides are the dominating phases at 5.4%O. As deoxidation proceeds, the newly reduced rare-earth metals combine with iron to form Fe-R metal compounds such as $Fe_{17}R_2$ and Fe_4RB_4. Eventually these compounds become the dominating phases.

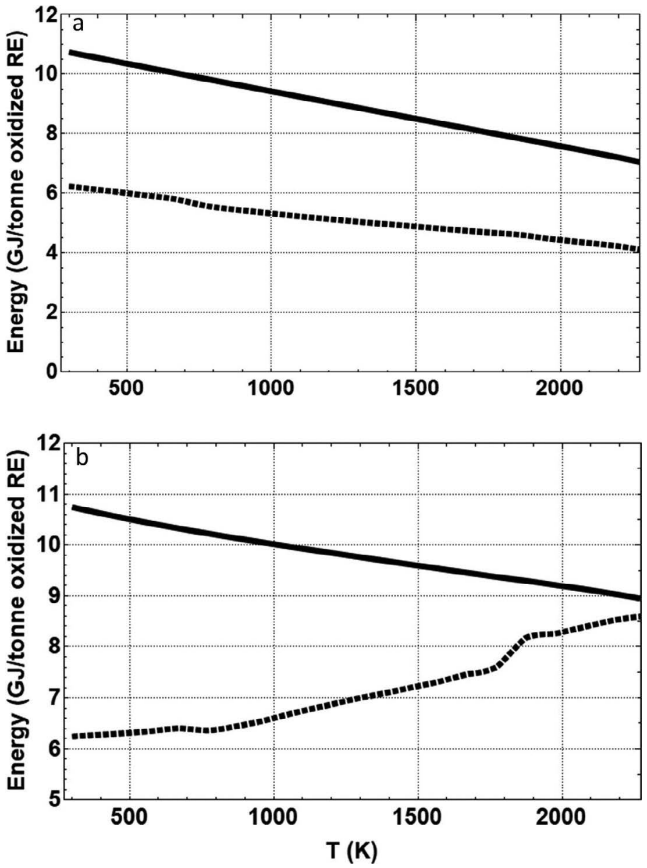

Fig. 9. a: minimum Gibbs energy (ΔG) needed to reduce equilibrated magnet sludge. b: minimum Gibbs energy (ΔG) to reduce magnet sludge with addition of the enthalpy (ΔH) to heat the material to temperature. –: modeled case where RE oxides are separated prior to treatment. ---: modeled case where sludge is reduced as a whole.

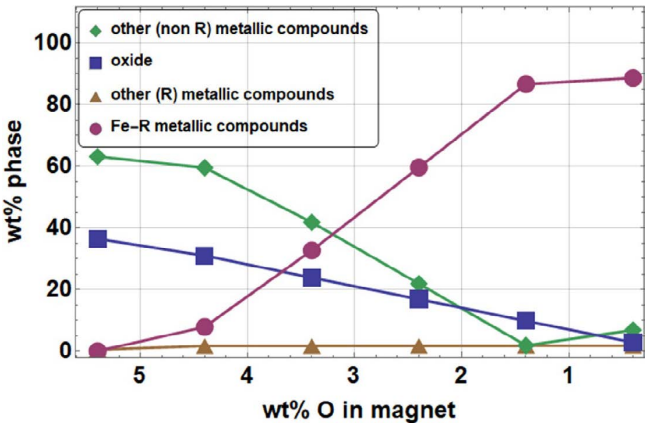

Fig. 10. Calculated changes in phases present as O content in magnet sludge is reduced from 5.4% to 0% at 1 773 K. ▲: rare-earth rich metallic phase (no Fe), ■: oxide phase , ●: metallic phases containing Fe and rare-earth, ♦: Fe-rich metallic phase (no rare-earth). As oxygen is removed, Fe and rare-earths interact to create new phases. (Online version in color.)

4. Discussion

4.1. Melting & Casting Model Performance

The initial, post-furnace composition of the magnet used in the simulation was estimated to contain 0.09% O and 0.02% C. This calculated oxygen level is below that reported for finished magnet products.[2,13] It has been observed that oxygen levels in a magnet increase during processing, particularly during the powder metallurgy steps.[24] Predicting a cast alloy oxygen content below the level in sintered magnets indicates sufficient performance of the proposed VIM model. The carbon level 0.02% was also just below the experimentally measured values of 0.03%.[13]

In order to produce a material with magnetic performances to the specifications of prior art, the 2-14 phase should comprise at least 80% of the rare-earth magnet by volume, and the "other metallic" grain boundary phase should be rare-earth rich.[1,22,25] A weight fraction of 90.63% for the 2-14 phase was predicted by the initial casting model. The "other metallic" phase predicted by the model was 82.5% rare-earth. Both the initial magnet composition and modeled phase distribution show good agreement with experimental data available in literature, supporting the validity of the casting model.

4.2. Oxidation Model Performance

The magnet oxidation model results in Fig. 7 show two important O compositions. First, at 0.8% O, the phase fraction of oxide overtakes the phase fraction of the grain boundary. In his study of NdFeB magnet recycling, Lalana noted both virgin and recycled magnets appear to reach an equilibrium oxygen concentration of 0.55%.[24] Kim *et al.* found that magnets with O levels greater than 0.6% showed a higher resistance to further oxidation.[32] These observations suggest a barrier preventing the magnet from easily uptaking oxygen near 0.55%–0.6%. The crossover near 0.8% in Fig. 7 indicates that such a barrier may be reproduced with the sole use of chemical thermodynamics.

The second important composition in Fig. 7 is at 1.8% O, above which the 2-14 composition breaks down significantly. It is well-documented that the 2-14 phase remains stable until a significant portion of the intergrain region has been oxidized. At this point the 2-14 phase decomposes into iron and rare-earth oxide.[24,25] The model results show a similar behavior, demonstrating agreement with experimental literature. A phase fraction of 80% by volume for the 2-14 phase is considered to be the threshold to achieve satisfactory magnet performance.[25] Past this threshold, the magnet likely becomes unusable and must be either sent to landfill or recycled alongside oxide feed at the smelter. Our chemical thermodynamic results thus explain the difficulties with recycling heavily oxidized magnet material.[3] Eventually, at 3.6%, most of the 2-14 phase has decomposed into rare-earth oxide and metallic iron.

The model's agreement with literature supports the utility of the weighted 2-14 phases. By lowering ΔH_{form} of 2-14 compounds until their formation was favored over competing ferrous intermetallics, the correct phase distribution was achieved without needing to "suppress" those intermetallic phases. This enabled them to re-emerge as oxygen content was increased and the 2-14 phase decomposed. If all competing phases were suppressed instead, the 2-14 phase would not decompose and the magnet would saturate in oxygen before reaching 5.4% O, an outcome in contradiction with literature.[11,13,30]

4.3. Implication for Magnet Sludge Recycling Technologies

The thermodynamic model has shown good agreement with available literature, both to reproduce melting and casting behavior at low oxygen content, and to predict the effects of higher oxygen content (oxidation) on magnet waste. With both low oxygen and high oxygen cases predicted solely by thermodynamic means, we can confidently extend such an approach to studying possible recycling pathways. In the most highly oxidized case of 5.4%O, rare-earth elements are only 30 wt% of the magnet, and 89% of the remaining material is iron. Although past recycling efforts have focused on processing the material from a rare-earth perspective, bearing in mind that magnet scrap is Fe-rich may offer new outlooks on its end of life treatment.

From a purely energetic standpoint, as shown in Fig. 9, less energy is needed to reduce the rare-earths if they are treated alongside the entire magnet material than to reduce only the rare-earth oxide. This benefit results from favorable interactions between iron and rare-earth metals. If only oxidized rare-earths are treated, no iron is present. Instead, if iron is kept, Fe-R compounds are quick to form as the rare-earth is deoxidized as shown in Fig. 10. The two competing reactions can be described as:

$$\left(Reaction\,1\right)\quad \frac{2}{y}R_xO_y \rightarrow \frac{2x}{y}R + O_2$$

$$\left(Reaction\,2\right)\quad \frac{2}{y}R_xO_y + zFe \rightarrow Fe_zR_{\frac{2x}{y}} + O_2$$

where $\Delta G_2 < \Delta G_1$ at the processing temperatures considered. It is important to note that at 1 773 K, the temperature of the deoxidation analysis in Fig. 10, the magnet should be mostly liquid.[24] Because herein we do not account for liquid solution behavior, there is no depression of the melting point and thus the model considers mostly solids alongside liquid compounds where the standard state melting temperature is below 1 773 K. For example, the stable form of pure iron at 1 773 K is BCC solid, and so all of the pure iron in the model at 1 773 K is considered to be BCC. It is well-known in thermodynamics that metals which are ordered compounds in the solid state immediately below their melting point will display short-range ordering at the stoichiometry of the compound in the liquid immediately above the melting point. Although $Fe_{17}R_2$ will not exist in the liquid state, favorable interactions between iron and rare-earth will remain after melting, and thus despite these approximations the model still informs trends in energy requirements during deoxidation.

Reducing the entire magnet material carries another benefit: no additional energy for mechanical or hydrometallurgical separation is required. This separation energy is significant. An estimated average 19.2 GJ/tonne RE is required to operate the hydrometallurgical pumps needed to separate rare-earth species to prepare them for molten salt electrolysis.[31] Including the cost of water treatment and the energy needed for solvent handling and consumption, LCA analyses for hydrometallurgical treatment have estimated a contribution of 58 GJ/tonne RE to the footprint of rare-earth processing.[33] We can calculate the energy required for molten salt electrolysis of one mole of RE metal using the Nernst equation:

$$\Delta G = -\frac{\Delta V}{nF}$$

where ΔV is estimated as a theoretical minimum of around 4.0 volts and the metal ion valency n is assumed to be 3.[31] A molar mass of 144.5 g/mol RE mix is calculated using the relative concentrations of Dy, Ce, Nd, Pr, La, and Gd present in this case study. This predicts a theoretical minimum of 8 GJ/ tonne RE required for electrolytic production of rare-earth metals.

Combining the theoretical minimum energy requirements for hydrometallurgical treatment (19.2 GJ) and for electrolysis (8 GJ) gives a total estimate of at least 27.2 GJ/tonne RE required for the traditional processing route shown in Fig. 3. This value can be compared to the range of 6–9 GJ/ tonne RE required for heating and reducing magnet sludge whole (Fig. 9). This estimate is similar in magnitude to the electrolysis minimum, suggesting that most of the energetic savings can be gained by avoiding elemental separation and hydrometallurgical treatment. **Figure 11** shows what such a direct processing route could look like.

Accounting for enthalpy, it can be seen in Fig. 9 that between 1 800 K and 1 900 K, ΔH increases with temperature due to melting and boiling of various elements. These results indicate an optimal temperature for a bulk magnet recycling process near 1 700 K, where the ΔG requirements are low but the ΔH costs have not yet started to sharply increase. **Table 3** compares the current sludge recycling process to the energetics needed to completely remove the oxygen from the magnet at 1 700 K. Eliminating the hydrometallurgical step and reducing the material directly would result in an estimated minimum energy saving of 78%.

The direct reduction of magnet sludge would be a streamlined “magnet-to-magnet” recycling method. Rather

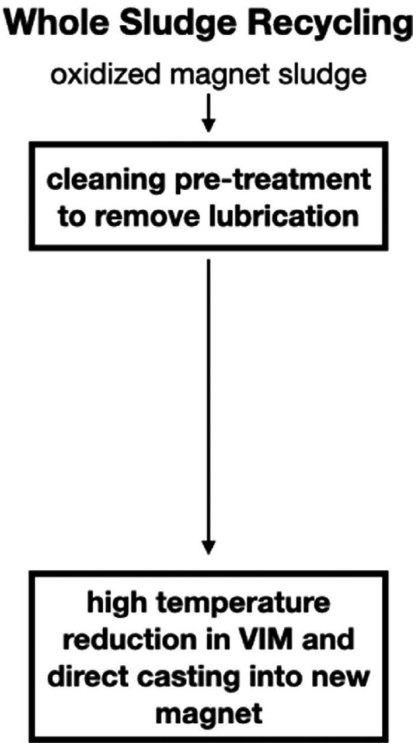

Fig. 11. Steps for direct recycling of magnet sludge.

Table 3. Comparison of theoretical energy needed for the current magnet sludge recycling method and the alternative of direct reduction of entire sludge without primary feed or elemental separation.

	Feedstock	Product	Process	Theoretical minimum energy (GJ/tonne)	Theoretical minimum energy (MWh/tonne)
Current method	magnet sludge and primary feed	individually purified, separate REEs	hydrometallurgical separation and molten salt electrolysis	27.2	7.6
Alternative method	magnet sludge	mixed RE and iron near proportions needed for magnet	direct reduction prior to vacuum melt and strip cast	7.5	2.1

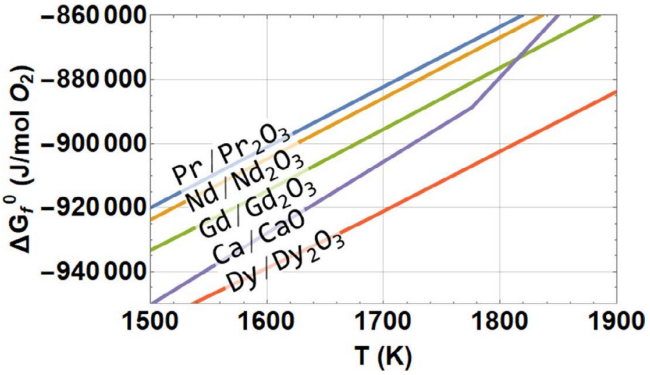

Fig. 12. Ellingham diagram showing the ΔG^0 of formation of relevant rare-earth oxides and calcium oxide, a popular choice for reductant in rare-earth recycling. ΔG^0_f is very similar for the various rare-earths, highlighting their chemical similarity and the resulting difficulty in purification from ore. (Online version in color.)

than completely break down and separate the waste into its 25+ elements, only to be re-mixed into a new magnet, one can envision a route (Fig. 11) where the waste is treated whole. Only minor elemental additions would be necessary to correct the stoichiometry to be commercially acceptable. Furthermore, the earlier optimal temperature, 1 700 K, is near the 1 723 K temperature used in the initial melting and casting step, and within the range proposed by various patents.[1,22,25] One can envision a unified process where the recycled material is reduced *in-situ* before being directly cast into a new magnet.

Metallothermic reduction is one common high-temperature deoxidation method. **Figure 12** shows the ΔG to reduce the rare-earths present in this case study. La and Ce, which require less energy to reduce, are not shown. The similarity in reduction energy among Pr, Nd, and Gd highlights the challenge in separating and purifying these elements. Ca, which has often been suggested as a possible reductant for rare-earth magnet recycling, is also pictured.[11,13] Dy cannot be reduced by Ca at 1 700 K. If Dy is left in an oxidized form and removed via slagging, there would be a loss of 14% of the total RE value.[34] In order to recover this value, the slag would need to be subjected to further processing, or an alternative to metallothermic reduction, such as electrolysis, should be considered. Electrochemical deoxidation has been shown to be an effective method at increasing the chemical potential of Ca so it can reduce Dy and other reactive rare-earths.[35]

5. Conclusions

Although rare-earth magnets are widespread in modern technology, their recycling methods are far from modern. Magnet sludge is often sent back to its primary processing feed and mixed with ore: all metallic material is oxidized via hydrometallurgy before being reduced and purified. Often, all this effort is expended only to re-mix the metals into a new magnet. In this work, a comprehensive thermodynamic study was run on the behavior of a magnet as it oxidizes, and the energy minimums to reduce sludge were estimated. In absence of a CALPHAD database for the 25+ elements typically found in a rare-earth magnet, a hybrid approach based in standard state classical thermodynamics was adopted. An energy saving of 78% was calculated if the separation and purification steps were skipped in favor of reducing the oxidized sludge whole.

REFERENCES

1) T. Onimura and S. Tabata: Method for Producing Alloy Cast Slab for Rare Earth Sintered Magnet, U. S. Patent US9862030B2, (2018).
2) E. Isotahdon: Ph.D. thesis, Tampere University of Technology, (2017), http://www.tut.fi/tutcris, (accessed 2020-01-18).
3) O. Takeda and T. H. Okabe: *Metall. Mater. Trans. E*, **1** (2014), 160. https://doi.org/10.1007/s40553-014-0016-7
4) J. C. K. Lee and Z. Wen: *J. Ind. Ecol.*, **21** (2017), 1277. https://doi.org/10.1111/jiec.12491
5) M. Zakotnik, E. Devlin, I. R. Harris and A. J. Williams: *J. Iron Steel Res. Int.*, **13** (2006), 289. https://doi.org/10.1016/S1006-706X(08)60197-1
6) A. Walton, H. Yi, N. A. Rowson, J. D. Speight, V. S. J. Mann, R. S. Sheridan, A. Bradshaw, I. R. Harris and A. J. Williams: *J. Clean. Prod.*, **104** (2015), 236. https://doi.org/10.1016/j.jclepro.2015.05.033
7) T. Uda, K. T. Jacob and M. Hirasawa: *Science*, **289** (2000), 2326. https://doi.org/10.1126/science.289.5488.2326
8) R. O. Suzuki, A. Saguchi, W. Takahashi, T. Yagura and K. Ono: *Mater. Trans.*, **42** (2001), 2492. https://doi.org/10.2320/matertrans.42.2492
9) S. Shirayama and T. H. Okabe: *Metall. Mater. Trans. B*, **49** (2018), 1067. https://doi.org/10.1007/s11663-018-1176-0
10) K. Asabe, A. Saguchi, W. Takahashi, R. O. Suzuki and K. Ono: *Mater. Trans.*, **42** (2001), 2487. https://doi.org/10.2320/matertrans.42.2487
11) A. Saguchi, K. Asabe, W. Takahashi, R. O. Suzuki and K. Ono: *Mater. Trans.*, **43** (2002), 256. https://doi.org/10.2320/matertrans.43.256
12) A. Saguchi, K. Asabe, T. Fukuda, W. Takahashi and R. O. Suzuki: *J. Alloy. Compd.*, **408–412** (2006), 1377. https://doi.org/10.1016/j.jallcom.2005.04.178
13) M. Yue, X. Yin, X. Li, M. Li, X. Li, W. Liu, Y. Wu, D. Zhang, J. Chen, X. Yi and T. Zuo: *ACS Sustain. Chem. Eng.*, **6** (2018), 6547. https://doi.org/10.1021/acssuschemeng.8b00358
14) A. Lixandru, P. Venkatesan, C. Jönsson, I. Poenaru, B. Hall, Y. Yang, A. Walton, K. Güth, R. Gauß and O. Gutfleisch: *Waste Manag.*, **68** (2017), 482. https://doi.org/10.1016/j.wasman.2017.07.028
15) B. Hallemans, P. Wollants and J. R. Roos: *J. Phase Equilib.*, **16** (1995), 137. https://doi.org/10.1007/BF02664851
16) M.-A. Van Ende, I.-H. Jung, Y.-H. Kim and T.-S. Kim: *Green Chem.*, **17** (2015), 2246. https://doi.org/10.1039/c4gc02232g
17) M.-A. Van Ende and I.-H. Jung: *J. Alloy. Compd.*, **548** (2013), 133. https://doi.org/10.1016/j.jallcom.2012.08.127
18) T. Chen, C. Guo, C. Li and Z. Du: *J. Magn. Magn. Mater.*, **497** (2020), 165983. https://doi.org/10.1016/j.jmmm.2019.165983
19) J. W. McMurray: *J. Am. Ceram. Soc.*, **99** (2016), 1092. https://doi.org/10.1111/jace.14049

20) B. Konar, J. Kim and I.-H. Jung: *Can. Metall. Q.*, **52** (2013), 321. https://doi.org/10.1179/1879139513Y.0000000080
21) L. K. Jakobsson, G. Tranell and I.-H. Jung: *Metall. Mater. Trans. B*, **48** (2017), 60. https://doi.org/10.1007/s11663-016-0748-0
22) S. Sasaki, H. Hasegawa and K. Nakajima: R-T-B Type Alloy, Production Method of R-T-B Type Alloy Flake, Fine Powder for R-T-B Type Rare Earth Permanent Magnet, and R-T-B Type Rare Earth Permanent Magnet, U. S. Patent US7846273B2, (2010).
23) C. W. Bale, E. Bélisle, P. Chartrand, S. A. Decterov, G. Eriksson, A. E. Gheribi, K. Hack, I. H. Jung, Y. B. Kang, J. Melançon, A. D. Pelton, S. Petersen, C. Robelin, J. Sangster, P. Spencer and M. A. Van Ende: *Calphad*, **54** (2016), 35. https://doi.org/10.1016/j.calphad.2016.05.002
24) E. Herraiz Lalana: Ph.D. thesis, University of Birmingham, (2016), https://etheses.bham.ac.uk/id/eprint/7609/, (accessed 2020-09-04).
25) S. Sasaki: Alloy Flake for Rare Earth Magnet, Production Method Thereof, Alloy Powder for Rare Earth Sintered Magnet, Rare Earth Sintered Magnet, Alloy Powder for Bonded Magnet and Bonded Magnet, International WO03/052778A1, (2003).
26) Wholesale Sponge Reduced Iron Powder Iron Price, Alibaba, https://www.alibaba.com/product-detail/wholesale-sponge-reduced-iron-powder-iron_60479474248.html?spm=a2700.7724838.2017115.187.f3ca5d42tC1ia3, (accessed 2020-01-28).
27) Low Carbon Ferroboron, Alibaba, https://www.alibaba.com/product-detail/Low-Carbon-FerroBoron_62400670208.html?spm=a2700.7724838.2017115.43.3aee6357dl7Qua, (accessed 2020-01-28).
28) Pr-Nd Master Alloy 7525 Praseodymium-Neodymium Metal, Alibaba, https://www.alibaba.com/product-detail/Pr-Nd-Master-Alloy-7525-Praseodymium_62121012293.html?spm=a2700.7724838.2017115.56.71dd6a0bZP60N4, (accessed 2020-01-28).
29) Airgas Product Catalog, Airgas, http://airgassgcatalog.com/catalog/, (accessed 2020-01-19).
30) K. Machida, M. Masuda, S. Suzuki, M. Itoh and T. Horikawa: *Chem. Lett.*, **32** (2003), 628. https://doi.org/10.1246/cl.2003.628
31) L. Talens Peiró and G. Villalba Méndez: *JOM*, **65** (2013), 1327. https://doi.org/10.1007/s11837-013-0719-8
32) A. S. Kim, F. E. Camp and E. J. Dulis: *IEEE Trans. Magn.*, **26** (1990), 1936. https://doi.org/10.1109/20.104576
33) P. S. Arshi, E. Vahidi and F. Zhao: *ACS Sustain. Chem. Eng.*, **6** (2018), 3311. https://doi.org/10.1021/acssuschemeng.7b03484
34) C. J. Berlet and K. Samnani: Rare Earth Metals, Mineral Prices, https://mineralprices.com/, (accessed 2020-01-14).
35) K. Hirota, T. H. Okabe, F. Saito, Y. Waseda and K. T. Jacob: *J. Alloy. Compd.*, **282** (1999), 101. https://doi.org/10.1016/S0925-8388(98)00807-X

Appendix 1. Chemical Thermodynamic Model for Baseline Case

Table A1. Chemical thermodynamic model for baseline case. Columns 1 and 2: initial elemental input into model including simulated Ar atmosphere. Columns 3 and 4: condensed phase output from model at 1 723 K, 0.5 bar. Columns 5 and 6: output from model at 298 K, 1 bar using "metastable assumptions" where pure C and Fe are suppressed, and weighted 2-14 compounds are used.

Input into "VIM model", 1 450C, 0.5 bar	g/tonne feedstock	Condensed phases stable at 1 723 K, 0.5 bar	g/tonne feedstock	Condensed phases metastable at 298 K, 1 bar	g/tonne cast product
Pr	66 873.35	Cu(liquid)	1 200.85	Ca3P2(solid)	31.69
Nd	234 633.66	Ga(liquid)	438.05	CTi(solid)	189.84
La	151.76	Pr(liquid)	52 212.64	Cr4C(solid)	50.64
Ce	151.76	CaC2(solid)	33.45	Mn7C3(solid)	271.12
Fe	650 572.86	CTi(solid)	189.84	Mn3Si(solid)	114.13
Al	6 597.03	Cr3C2(solid)	55.25	Mn5Si3(solid)	176.35
Si	58.01	Mn7C3(solid)	71.02	CoAl(solid)	6 472.52
Mo	151.76	Mn5Si3(solid)	247.13	Cu(solid)	874.54
W	151.76	Mn2P(solid)	290.09	Cu3P(solid)	379.34
Ti	151.76	CoAl(solid)	6 472.52	Ga(solid)	438.05
Ca	30.35	Nb8C7(solid)	558.42	Nb8C7(solid)	558.42
Mg	102.22	MoB(solid)	168.86	MoB(solid)	168.86
S	96.96	LaC2(solid)	178.01	LaC2(solid)	178.01
C	176.53	Ce2C3(solid)	171.28	Ce2C3(solid)	171.28
B	9 582.00	PrAl2(solid)	16 482.46	Pr(solid)	54 954.80
P	63.88	Gd2O3(solid)	87.94	PrAl2(solid)	16 482.46
Mn	587.54	GdS(solid)	572.47	Nd(solid)	860.53
Cr	47.91	Dy2O3(solid)	7 074.04	Nd2O3(solid)	6 381.50
O	921.98	TaC(solid)	0.42	Gd2O3(solid)	87.94
Nb	501.68	WC(solid)	161.68	GdS(solid)	572.47
Ta	0.39	Fe4PrB4(solid)	7 416.67	TaC(solid)	0.42
Dy	16 655.63	Fe4NdB4(solid)	158.89	WC(solid)	161.68
Gd	551.84	Fe14Nd2B(solid)	879 130.83	Fe14Nd2B(solid)	844 232.07
Co	4 439.83	Fe3Dy(solid)	21 285.66	Fe14Dy2B(solid)	57 240.60
Cu	1 204.02			B5Nd2(solid)	3 609.23
Ga	501.68				
Zn	5 041.84				
Ar	1 254.855				
O2	0.001				
H2O	0.001				
CO2	0.001				
N2	0.004				

Appendix 2. Chemical Thermodynamic Model for Case where O Content is 0.1%

Table A2. Chemical thermodynamic model for case where O content is 0.1%. Columns 1 and 2: Initial elemental composition obtained from baseline model. Columns 3 and 4: input into model using rescaled composition to achieve 0.1%O while keeping the relative concentration of all other elements constant. Columns 5 and 6: output from model at 298 K, 1 bar using "metastable assumptions" where pure C and Fe are suppressed, and weighted 2-14 compounds are used.

Starting elemental composition ("Post-VIM")	g/tonne cast	Elemental composition rescaled to contain 0.1% O	g/tonne cast	Condensed phases metastable at 298 K, 1 bar, 0.1%O	g/tonne cast
Pr	67 232.10	Pr	67 227.19	Ca3P2(solid)	31.86
Nd	235 891.79	Nd	235 874.53	CTi(solid)	190.85
La	152.58	La	152.57	Cr4C(solid)	50.91
Ce	152.58	Ce	152.57	Mn7C3(solid)	272.56
Fe	654 066.46	Fe	654 018.61	Mn3Si(solid)	114.73
Al	6 632.40	Al	6 631.92	Mn5Si3(solid)	177.28
Si	58.32	Si	58.32	CoAl(solid)	6 506.80
Mo	152.58	Mo	152.57	Cu(solid)	879.17
W	152.58	W	152.57	Cu3P(solid)	381.35
Ti	152.58	Ti	152.57	Ga(solid)	440.37
Ca	21.03	Ca	21.02	Nb8C7(solid)	561.38
S	97.48	S	97.47	MoB(solid)	169.75
C	177.47	C	177.45	LaC2(solid)	178.95
B	9 633.46	B	9 632.76	Ce2C3(solid)	172.18
P	64.14	P	64.13	Pr(solid)	55 245.88
Mn	482.94	Mn	482.90	PrAl2(solid)	16 569.76
Cr	48.14	Cr	48.13	Nd(solid)	425.31
O	926.90	O	1 000	Nd2O3(solid)	6 928.24
Nb	504.37	Nb	504.33	Gd2O3(solid)	88.41
Ta	0.40	Ta	0.40	GdS(solid)	575.50
Dy	16 733.59	Dy	16 732.36	TaC(solid)	0.42
Gd	554.77	Gd	554.73	WC(solid)	162.53
Co	4 463.67	Co	4 463.34	Fe14Nd2B(solid)	848 703.67
Cu	1 207.30	Cu	1 207.21	Fe14Dy2B(solid)	57 543.78
Ga	440.40	Ga	440.37	B5Nd2(solid)	3 628.35